Publ. Astron. Soc. Japan (2018) 70 (1), 6 (1–10)
doi: 10.1093/pasj/psx152

Detection of the thermal component in GRB 160107A

Yuta KAWAKUBO,[1,*] Takanori SAKAMOTO,[1] Satoshi NAKAHIRA,[2] Kazutaka YAMAOKA,[3] Motoko SERINO,[1] Yoichi ASAOKA,[4] Michael L. CHERRY,[5] Shohei MATSUKAWA,[1] Masaki MORI,[6] Yujin NAKAGAWA,[7] Shunsuke OZAWA,[4] Ana V. PENACCHIONI,[8,9] Sergio B. RICCIARINI,[10] Akira TEZUKA,[1] Shoji TORII,[4] Yusuke YAMADA,[1] and Atsumasa YOSHIDA[1]

[1]Department of Physics and Mathematics, Aoyama Gakuin University, 5-10-1 Fuchinobe, Chuo-ku, Sagamihara, Kanagawa 252-5258, Japan
[2]MAXI team, RIKEN, 2-1 Hirosawa, Wako, Saitama 351-0198, Japan
[3]Institute for Space-Earth Environmental Research (ISEE), Nagoya University, Furo-cho, Chikusa-ku, Nagoya, Aichi 464-8601, Japan
[4]Research Institute for Science and Engineering, Waseda University, 3-4-1 Okubo, Shinjuku, Tokyo 169-8555, Japan
[5]Department of Physics and Astronomy, Louisiana State University, 202 Nicholson Hall, Baton Rouge, LA 70803, USA
[6]Department of Physical Sciences, College of Science and Engineering, Ritsumeikan University, 1-1-1 Noji-higashi, Kusatsu, Shiga 525-8577, Japan
[7]Center for Earth Information Science and Technology, Japan Agency for Marine-Earth Science and Technology, 3173-25 Showa-machi, Kanazawa-ku, Yokohama, Kanagawa 236-0001, Japan
[8]Department of Physical Science, Earth and Environment, University of Siena, via Roma 56, 53100, Siena, Italy
[9]ASI Science Data Center (ASDC), Via del Politecnico snc, 00133 Rome, Italy
[10]Institute of Applied Physics (IFAC), National Research Council (NRC), Via Madonna del Piano, 10, 50019 Sesto, Fiorentino, Italy

*E-mail: ykawakubo@phys.aoyama.ac.jp

Received 2017 October 2; Accepted 2017 December 7

Abstract

We present the detection of a blackbody component in gamma-ray burst GRB 160107A emission by using the combined spectral data of the CALET Gamma-ray Burst Monitor (CGBM) and the MAXI Gas Slit Camera (GSC). MAXI/GSC detected the emission ∼45 s prior to the main burst episode observed by the CGBM. The MAXI/GSC and the CGBM spectrum of this prior emission period is fitted well by a blackbody with temperature $1.0^{+0.3}_{-0.2}$ keV plus a power law with a photon index of -1.6 ± 0.3. We discuss the radius of the photospheric emission and the main burst emission based on the observational properties. We stress the importance of coordinated observations via various instruments collecting high-quality data over a broad energy coverage in order to understand the GRB prompt emission mechanism.

Key words: gamma-ray burst: general — gamma-ray burst: individual (GRB 160107A) — radiation mechanisms: non-thermal — radiation mechanisms: thermal

1 Introduction

Gamma-ray bursts (GRBs) are short (from a few ms up to ∼100 s) and intense flashes of gamma-rays; they are classified into short GRBs and long GRBs depending on whether their durations are shorter or longer than 2 s (Kouveliotou et al. 1993). It is widely accepted that these two GRB populations originate from different progenitors. The long GRBs are the result of explosions of massive stars (e.g., Woosley & Bloom 2006), while the short GRBs are due to mergers of two neutron stars or to neutron star–black hole binaries (Eichler et al. 1989; Paczynski 1991; Narayan et al. 1992). Merger events have been shown to be gravitational wave sources detectable by the current generation of detectors such as the Laser Interferometer Gravitational-Wave Observatory (LIGO) and Virgo (Abbott et al. 2016, 2017).

The radiation processes for prompt GRB emission are still far from being understood. Most GRB prompt emission spectra are well represented by a smoothly connected broken power-law function–Band function (Band et al. 1993). The break energies, $E_{\rm peak}$ (the peak energy in the νF_ν spectrum), are broadly distributed from a few keV up to a few MeV (Sakamoto et al. 2005). This broad $E_{\rm peak}$ distribution reflects the intrinsic properties of GRB spectra (e.g., Amati et al. 2002); its origin is not clear. Although the observed spectrum is due to the synchrotron radiation from relativistic electrons (e.g., Tavani 1996), the low-energy photon indices of some of the observed spectra show a harder index than expected from synchrotron radiation (e.g., Preece et al. 1998). A unique observation is needed to break through the current situation.

One interesting characteristic seen in some GRBs is the emergence of thermal emission in the prompt GRB spectra (e.g., Frontera et al. 2001). The spectrum of the prompt emission of GRB 041006 shows blackbody components superimposed on the non-thermal spectrum (Shirasaki et al. 2008) with time-averaged temperatures of 0.2 and 0.4 keV. Starling et al. (2012) identified a blackbody component with temperature between 0.1 and 1 keV in the Swift data for nine GRBs. Identifications of the blackbody component with temperatures of several tens of keV up to 100 keV are claimed by the BATSE and Fermi/GBM data (Ryde 2005, 2010; Guiriec et al. 2013). Although thermal emission from the photosphere is expected in the standard fireball model (Goodman 1986; Paczynski 1986), the wide dynamic range of the claimed blackbody temperature distribution in the spectra observed in prompt GRB is difficult to understand in a simple way.

The CALorimetric Electron Telescope (CALET) was attached to the Exposed Facility of the Japanese Experimental Module (JEM) on the International Space Station (ISS) in 2015 August (Torii et al. 2011). The main scientific goals of CALET are observations of high-energy cosmic electrons and high-energy GeV–TeV gamma-rays thanks to its thick calorimeter. To support the gamma-ray observations, CALET includes the CALET Gamma-ray Burst Monitor (CGBM) to observe prompt emissions of GRBs (Yamaoka et al. 2013). After a month of initial checkout, CGBM began its scientific observation in 2015 October; it consists of two kinds of scintillation detectors to cover a wide energy range from 7 keV up to 20 MeV: (1) The Hard X-ray Monitor (HXM) consists of a $LaBr_3$(Ce) crystal (61 mm diameter and 1.27 mm thickness) with a 410 μm thickness Be window and a photomultiplier tube (PMT) covering the energy range from 7 keV to 1 MeV. There are two identical HXM units (HXM1 and HXM2) facing in the same direction tilted roughly 10° from the zenith direction. (2) The other scintillator is the Soft Gamma-ray Monitor (SGM), utilizing a BGO crystal (102 mm in diameter and 76 mm in thickness) and a PMT to cover the energy range from 40 keV to 20 MeV. The SGM points in the zenith direction. The fields of view of HXM and SGM are ∼120° and ∼2π sr. The GRB detection rate of CGBM is ∼4 GRBs per month.

The Monitor of All-sky X-ray Image (MAXI) is also mounted on the Exposed Facility of the JEM-ISS (Matsuoka et al. 2009); it consists of two different slit cameras: the Gas Slit Camera (GSC) and the Solid-state Slit Camera (SSC), consisting of one-dimensional position-sensitive proportional counters and X-ray CCDs respectively. GSC covers the energy range of 2–30 keV and the two instantaneous fields of view of 1°.5 × 160° at the zenith and the horizontal direction of the ISS. Because CALET and MAXI sit on the same platform, most of the MAXI/GSC and CGBM fields of view overlap.

In this paper, we report on the prompt emission properties of GRB 160107A. In subsection 2.1, the temporal results from the CGBM and the MAXI/GSC data, and also the localization by the MAXI/GSC and the Interplanetary Network, are shown. We present the CGBM and the MAXI/GSC spectral properties in subsection 2.2. We discuss our results in section 3. The quoted errors are at the 90% confidence level unless stated otherwise.

2 Observation and data analysis

2.1 Temporal properties and localization

GRB 160107A was detected by CGBM on 2016 January 7 at 22:20:43.20 (UT) (Nakahira et al. 2016). The burst was also detected by MAXI/GSC (Nakagawa et al. 2016), Fermi/GBM (Veres et al. 2016), INTEGRAL (SPI-ACS), and Wind/KONUS (Golenetskii et al. 2016). Figure 1 shows

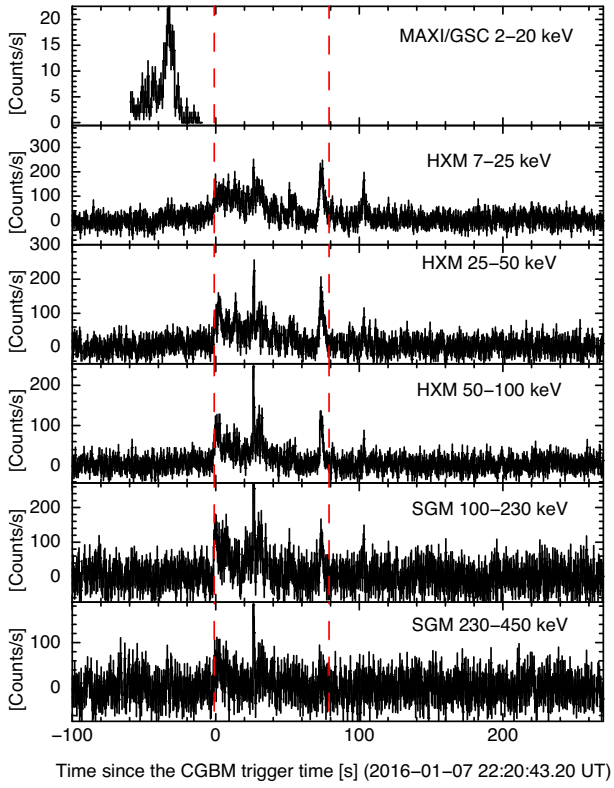

Fig. 1. The 1 s binning light curves of GRB 160107A observed by MAXI and CGBM. The red dashed lines show the time interval of the time-averaged spectrum. The MAXI light curve (top panel) is not corrected for the time-variable effective area. (Color online)

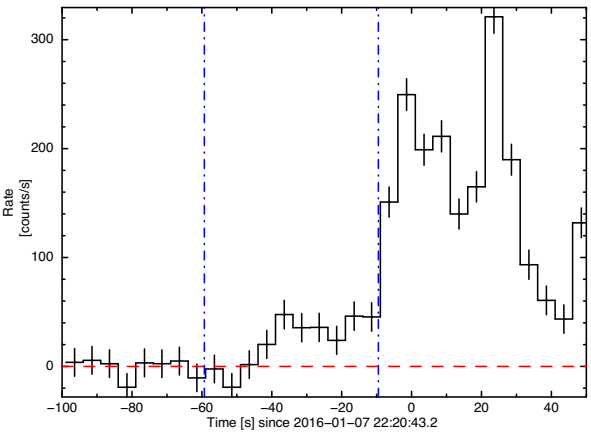

Fig. 2. The 5 s binned HXM light curve of GRB 160107A (7–100 keV). A red dashed line shows the background level. The blue dot-dashed lines represent the observation time window of MAXI. The prior emission observed by MAXI is visible in the HXM light curve. (Color online)

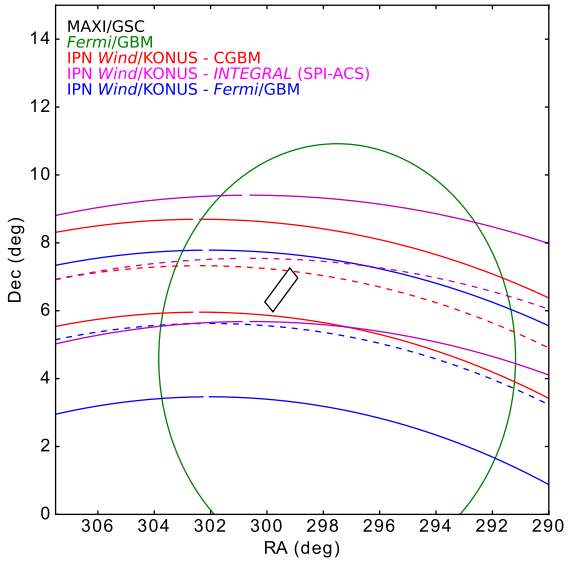

Fig. 3. Localization of GRB 160107A. The black and green lines represent the MAXI/GSC error box and Fermi/GBM error circle, respectively. The red, magenta, and blue lines show the IPN localizations of Wind/KONUS–CGBM, Wind/KONUS–INTEGRAL (SPI-ACS), and Wind/KONUS–Fermi/GBM, respectively. (Color online)

the light curve of GRB 160107A based on the CGBM and MAXI/GSC data. The CGBM light curve shows a complex structure with multiple overlapping pulses. We use the Swift analysis tool, `battblocks`, to measure the T_{90} of the SGM data. The no-background subtracted light curve in 0.125 s binning over the 40–1000 keV band is used. The T_{90} measured by the SGM is 73.5 ± 19.0 s (1σ). Thus, GRB 160107A is classified as a long GRB. Interestingly, as seen in figure 1, the emission seen by MAXI/GSC was ~45 s earlier than the CGBM trigger time. At the time of the MAXI detection, a faint emission is visible in the HXM light curve (figure 2). The significance of this weak emission in the HXM is 5.5σ in the 7–100 keV band. Note that the field of view of the MAXI/GSC camera moved outside the location of GRB 160107A around 20 s before the CGBM trigger time. Therefore, the main part of the emission was not detected by MAXI/GSC.

The best-fit 90% error region based on the MAXI/GSC data is described by a rectangular region with the following four corners: (RA, Dec) = (298.°905, 6.°966), (299.°190, 7.°260), (300.°076, 6.°261), and (299.°789, 5.°968)(J2000.0). The Fermi/GBM ground localization is (RA, Dec) = (297.°510, +4.°590)(J2000.0) with a 2.°6 error radius (1σ) plus a systematic error of ~ 3.°7 (Connaughton et al. 2015), which is consistent with the MAXI/GSC error region. We further performed localization analysis using the Interplanetary Network (IPN). We cross-correlated the light curve data of Fermi/GBM and Wind/Konus, and SGM and Wind/Konus, and INTEGRAL (SPI-ACS) and Wind/Konus. Figure 3 shows the IPN position annuli overlaid with the MAXI/GSC and the Fermi/GBM best positions. The IPN location is consistent with the MAXI/GSC error region, but the MAXI/GSC error region provides the best localization of this GRB. Based on the temporal and the positional coincidence, we concluded

Table 1. Time-averaged spectral parameters of the CGBM spectrum.

Model	α	β	$E_{\rm peak}$ [keV]	A* [ph cm^{-2} s^{-1} keV^{-1}]	SGM constant factor	χ^2/d.o.f.
PL†	-2.1 ± 0.1	–	–	67^{+39}_{-24}	$1.33^{+0.31}_{-0.27}$	54.04/49
CPL‡	$-1.7^{+0.3}_{-0.2}$	–	102^{+48}_{-40}	19^{+28}_{-12}	$1.42^{+0.31}_{-0.27}$	45.62/48
BAND§	$-1.8^{+0.2}_{-0.3}$	-2.3 (fixed)	94^{+74}_{-83}	$6.0^{+2.8}_{-1.0} \times 10^{-3}$	$1.35^{+0.29}_{-0.26}$	48.92/48

*The normalization of the power-law and cutoff power-law models was calculated at 1 keV, whereas the normalization of the Band function was calculated at 100 keV.
†A power-law model.
‡A power-law times exponential cutoff model.
§Band function.

that the MAXI/GSC emission is clearly associated with GRB 160107A.

2.2 Spectrum

First, we investigated the spectral properties of the main part of the emission using the CGBM data. The spectral files extracting the data between $T_0 - 1.1$ s and $T_0 + 78.9$ s were created for HXM1, HXM2, and SGM, where T_0 is the trigger time of CGBM (January 7 at 22:20:43.20). The background files were generated for each spectral channel by fitting the channel separately with a second-order polynomial function before the burst ($T_0 - 269.1$ s to $T_0 - 81.1$ s) and after the burst ($T_0 + 230.9$ s to $T_0 + 798.9$ s). Gain correction was applied to those spectral files by fitting the background lines at 1.47 MeV due to ^{138}La in the $LaBr_3$(Ce) crystal for the HXM data (Quarati et al. 2012) and 2.2 MeV due to activation of the BGO crystal for the SGM data. We examined the gain-corrected spectra using the background lines at 35.5 keV and 511 keV, and found the energy of those lines to be accurate within 5%. The detector response matrices (DRMs) of CGBM were developed using a Monte Carlo simulator based on the GEANT4 software package (Agostinelli et al. 2003). Since the DRMs are sensitive to the incident angle of the event, we ran the simulator using the best burst position from MAXI, (RA, Dec) = (299.°670, 6.°413) (J2000.0). The incident angles of GRB 160107A at the detector plane of HXM and SGM were $(\theta, \phi) = (23.°2, 174.°6)$ and $(13.°3, 170.°6)$, where θ and ϕ are the zenith and azimuth angles. The zenith direction of CALET corresponds to $\theta = 0°$. The front direction of CALET corresponds to $\phi = 0°$. Since the variation in the incident angle θ during the burst interval ($\sim$80 s) is less than $\sim 1.°5$, we used the DRM for the fixed position. Details of the CGBM DRMs, the calibration status, and the results of the cross-spectral calibrations using simultaneously detected bright GRBs with the Swift/BAT data are described in appendices 1 and 2. Since there is uncertainty due to absorption by structures around detectors in the low-energy region, we only used the data above 30 keV for HXM and above 100 keV for SGM. XSPEC version 12.9.1 is used in the spectral analysis.

Table 1 presents the results of the time-integrated spectral analysis of the burst. The spectrum is fitted best by a power law times an exponential cutoff (CPL) function. The χ^2 improvement in a CPL over a simple power-law (PL) fit is 8.42 in 1 degree of freedom. A Band function results in no better χ^2 than CPL. We simulated 10000 spectra, inputting the best-fit parameters of a CPL model using the same background spectrum generated in the analysis. We fitted the simulated spectra by both PL and CPL models, and calculated the number of simulated spectra that exceeded a $\Delta\chi^2$ [$= \chi^2$(CPL) $- \chi^2$(PL)] of 8.42. We found that 4459 simulated spectra exceeded $\Delta\chi^2$ of 8.42. This corresponds to an improvement significance of 44.6%. Therefore, the improvement in χ^2 of CPL over PL in the observed spectrum was not highly significant based on the simulation study. However, the best-fit photon index α of $-1.7^{+0.3}_{-0.2}$ and $E_{\rm peak}$ of 102^{+48}_{-40} keV in the CPL model are consistent with Wind/KONUS and Fermi/GBM (Gruber et al. 2014; von Kienlin et al. 2014; Golenetskii et al. 2016; Narayana Bhat et al. 2016), with α steeper than typical values of the low-energy photon index for long GRBs (Kaneko et al. 2006). The fluence and the 1 s peak flux calculated in the best fit CPL were $1.6 \pm 0.1 \times 10^{-5}$ erg cm^{-2} (1σ) and $1.6 \pm 0.1 \times 10^{-6}$ erg cm^{-2} s^{-1} (1σ) in the 30–500 keV band. The 1 s peak flux was measured between $T_0 + 26.2$ s and $T_0 + 27.2$ s. The results can be seen in figure 4.

Next, we examined the MAXI/GSC spectrum at the time of the MAXI detection. We used the MAXI standard software for creating the spectrum. The calibrated MAXI/GSC event data were downloaded from the Data Archive Transmission System (DARTS: Tamura et al. 2004).[1] The MAXI/GSC cameras ID 4 and 5 detected the photons from the GRB. After the observation information files were generated by `mxscancur`, the exposure maps (WMAP files) for the individual cameras were created by

[1] ⟨http://darts.isas.jaxa.jp/pub/maxi⟩.

mxgtiwmap. The source and the background spectral files were extracted by xselect from the calibrated MAXI/GSC event file. The source region was selected as a circle of radius 1°.6 centered at (RA, Dec) = (299°.670, 6°.413) (J2000.0). The background region was an annulus of outer radius 3° and inner radius 1°.6 centered at (RA, Dec) = (299°.670, 6°.413) (J2000.0). There is ∼10% uncertainty in the exposure time due to the position uncertainty. The source spectrum was extracted when the effective area to the source position was $>0.05\,\mathrm{cm}^2$, which corresponds to from $T_0 - 59.3$ s to $T_0 - 9.5$ s. The detector response files were generated by mxgrmfgen. The energy range used in the spectral analysis of the MAXI/GSC spectrum was from 2 keV to 30 keV. There was no issue of the dead-time in the MAXI/GSC data in the count rate level of GRB 170107A.

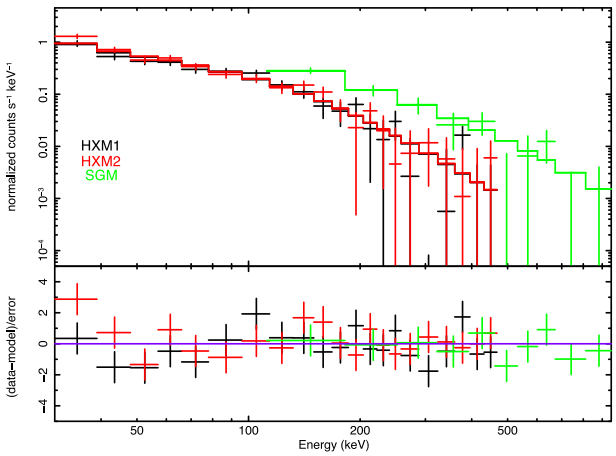

Fig. 4. CGBM time-averaged spectrum of GRB 160107A. The black, red, and green points are the HXM1, HXM2, and the SGM data, respectively. The best-fit model is a CPL. (Color online)

Table 2 shows the results of the spectral analysis of the MAXI prior emission. We fitted the spectrum by a power law, a blackbody, a cutoff power law, a Band function, and a power law plus blackbody model with the interstellar absorption, N_{H}, which is the model "wabs" in xspec. The best-fit spectral model for the MAXI/GSC data was the highly absorbed power-law model with $N_{\mathrm{H}} = 3.7^{+3.2}_{-2.6} \times 10^{22}\,\mathrm{cm}^{-2}$. However, we believe this best-fit model is unphysical because of the unrealistically large N_{H}. This GRB is located at the galactic latitude of −12° and the Galactic N_{H} calculated by Dickey and Lockman (1990) at this direction is $1.4 \times 10^{21}\,\mathrm{cm}^{-2}$. Furthermore, according to Willingale et al. (2013), the mean observed N_{H} of X-ray afterglow spectra observed by Swift XRT is $2.1 \times 10^{21}\,\mathrm{cm}^{-2}$. Our derived N_{H} of $3.7 \times 10^{22}\,\mathrm{cm}^{-2}$ corresponds to 4.7×10^{-3} percentile of the N_{H} distribution of Willingale et al. (2013). Therefore, we concluded that the absorption-like feature apparently seen at low energy in the MAXI/GSC spectrum is not due to real absorption by the interstellar medium and the host galaxy of GRB 160107A. On the other hand, although a residual is seen at high energies, the spectrum can be also be fitted well by a blackbody with temperature 1.2 keV. It is possible to reduce this residual in the blackbody fit by adding

Table 2. Fit parameters for the MAXI prior emission spectrum.

Instruments	Model	nH [$10^{22}\,\mathrm{cm}^{-2}$]	α	β	E_{peak} [keV]	A_{PL}* [ph cm^{-2} s^{-1} keV^{-1}]	kT [keV]	A_{BB}†	χ^2/d.o.f.
MAXI	PL§	$3.7^{+3.2}_{-2.6}$	$-2.7^{+0.6}_{-0.8}$	–	–	12^{+35}_{-8}	–	–	9.18/9
MAXI	PL	0.14 (fixed)	-2.0 ± 0.2	–	–	$2.8^{+1.2}_{-0.9}$	–	–	14.64/10
MAXI	BB‖	0.14 (fixed)	–	–	–	–	1.2 ± 0.2	0.11 ± 0.01	21.21/10
MAXI	CPL♯	0.14 (fixed)	$-1.2^{+1.4}_{-0.9}$	–	>2	$1.9^{+1.6}_{-1.0}$	–	–	13.03/9
MAXI	BAND**	0.14 (fixed)	$+1.8^{+0.6}_{-2.5}$	$-2.4^{+0.4}_{-0.6}$	<5	<124	–	–	8.49/8
MAXI	PL+BB	0.14 (fixed)	$-0.6^{+3.5}_{-1.2}$	–	–	$0.09^{+1.67}_{-0.09}$	1.0 ± 0.2	$0.08^{+0.03}_{-0.05}$	8.45/8
MAXI	PL+BB	0.14 (fixed)	−1.0 (fixed)	–	–	0.2 ± 0.1	0.9 ± 0.2	0.07 ± 0.02	8.57/9
MAXI & HXM	PL	0.14 (fixed)	-1.9 ± 0.2	–	–	$2.6^{+1.0}_{-0.7}$	–	–	16.83/14
MAXI & HXM	BB	0.14 (fixed)	–	–	–	–	1.2 ± 0.2	0.11 ± 0.01	31.83/14
MAXI & HXM	CPL	0.14 (fixed)	−1.88‡	–	Not determined	2.6‡	–	–	16.84/13
MAXI & HXM	BAND	0.14 (fixed)	$+1.7^{+0.6}_{-3.2}$	$-2.1^{+0.2}_{-0.4}$	<6	56^{+51}_{-56}	–	–	13.47/12
MAXI & HXM	PL+BB	0.14 (fixed)	-1.6 ± 0.3	–	–	$0.9^{+1.2}_{-0.6}$	$1.0^{+0.3}_{-0.2}$	$0.05^{+0.03}_{-0.04}$	11.73/12

*Normalization of either a power law or a power law times exponential cutoff model at 1 keV; the normalization of the Band function was calculated at 10 keV.
†Normalization of a blackbody in units of L_{39}/D_{10}^2, where L_{39} is the source luminosity in units of 10^{39} erg s^{-1} and D_{10} is the distance of the source in units of 10 kpc.
‡An error is not available.
§A power-law model.
‖A blackbody.
♯A power law times exponential cutoff model.
**Band function.

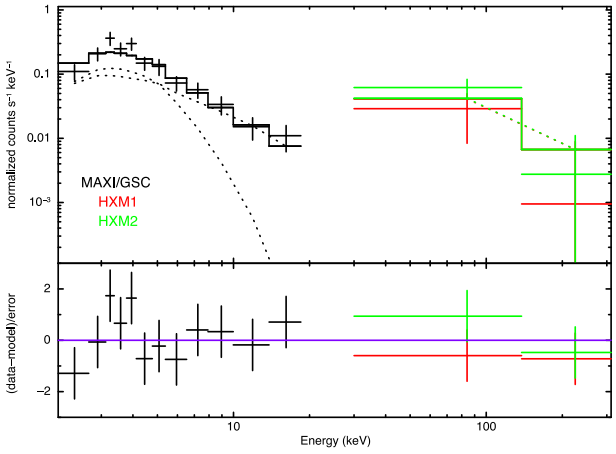

Fig. 5. Time-averaged spectrum of the prior emission with a best-fit PL + BB model. The black, red, and green points are the MAXI/GSC, the HXM1, and the HXM2 data, respectively. The best-fit model is PL + BB. (Color online)

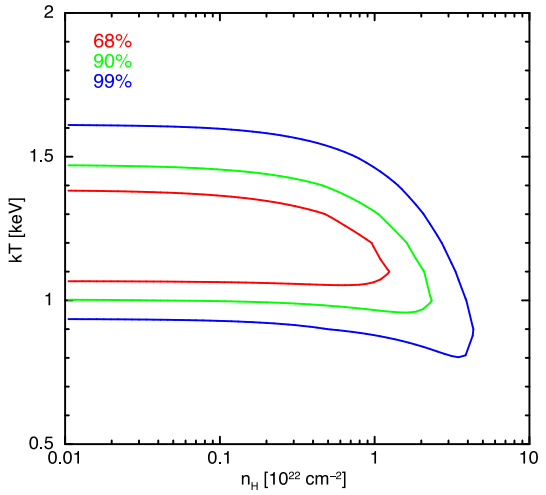

Fig. 6. Confidence contour between a blackbody temperature and $N_{\rm H}$ at the spectrum of the prior emission interval. (Color online)

a power-law component. No significant improvement in χ^2 was seen by the Band function over a simple power-law fit.

We also performed a joint fitting analysis including the HXM data. The time interval of the HXM spectrum was between $T_0 - 61.0$ s and $T_0 - 13.1$ s. The results of the joint fitting are shown in table 2 and figure 5. We found that the best-fit spectral model was a blackbody plus a power-law model in the joint fit analysis. The photon index of $\alpha = -1.6 \pm 0.3$ and temperature of $kT = 1.0^{+0.3}_{-0.2}$ keV are consistent with the results from the MAXI/GSC data alone. The χ^2 improvement of an absorbed blackbody plus a power-law model over an absorbed power-law model is 5.10 in 2 degrees of freedom. We simulated 10000 spectra, inputting the best-fit parameters of an absorbed blackbody plus a power-law model. We fitted the simulated spectra by both an absorbed blackbody plus a power-law model and an absorbed power-law model, and calculated the number of simulated spectra that exceeded a $\Delta\chi^2$ of 5.10. We found that 3056 simulated spectra exceeded a $\Delta\chi^2$ of 5.10. The significance of the improvement is 30.6%. In addition to the discussion regarding $N_{\rm H}$ in the previous paragraph, the best representative model ofthe prior emission spectrum was a blackbody plus a power-law model, with the thermal emission superimposed on the non-thermal component at ∼45 s before the main burst episode. As shown in figure 6, our derived blackbody temperature is not sensitive to the value of $N_{\rm H}$.

3 Discussion

The MAXI/GSC detection prior to the main burst episode was achieved in coordination with the high-sensitivity soft X-ray survey data of MAXI/GSC and the wide-field hard X-ray survey data of CGBM, both of which are physically located on the same platform. CGBM provides the data from 7 keV up to 20 MeV for a bright transient source, whereas MAXI/GSC provides simultaneous data from 2 keV up to 30 keV. The field of view of the MAXI/GSC cameras always overlap with that of the CGBM. Therefore, we would expect to have GRBs observed simultaneously by CGBM and MAXI/GSC. We estimate the number of simultaneously observed GRBs as follows: The instantaneous fields of view of the SGM and the MAXI/GSC are 20000 deg^2 ($\sim 2\pi$) and 480 deg^2 ($1.^\circ 5 \times 160^\circ$ in two directions). The observation efficiencies are 40% for the MAXI/GSC (Sugizaki et al. 2011) and 60% for the CGBM. Since the CGBM detects ∼50 GRBs per year, we expect ∼1 GRB per year to be detected simultaneously. However, as we show here for GRB 160107A, the timing is not necessarily matched between the two instruments. Furthermore, to confirm this fact, MAXI/GSC also detected the emission at 320 s after the main burst episode for GRB 160509A (Ono et al. 2016). So far, we have four simultaneously detected GRBs between the CGBM and MAXI/GSC in one year of overlapping operation.

Following the argument of Pe'er (2007), we estimated the photospheric radius from the observed parameters of the blackbody component. The photospheric radius $R_{\rm ph}$ can be estimated by the following equation: $R_{\rm ph} = \gamma_0\, d_{\rm L}\, \mathcal{R}/\xi\, (1+z)^2$, where γ_0 is the bulk Lorentz factor, $d_{\rm L}$ is the luminosity distance, ξ is a geometric factor of order unity (we assume $\xi = 1$), z is the redshift, and $\mathcal{R}$ [$\equiv (F_{\rm BB}/\sigma\ T_{\rm BB}^4)^{0.5}$] is the ratio between the blackbody flux $F_{\rm BB}$ and $\sigma\ T_{\rm BB}^4$, where σ is the Stefan–Boltzmann constant and $T_{\rm BB}$ is the blackbody temperature. From the observed blackbody component, we derived $\mathcal{R} = 2.9 \times 10^{-17}$. Assuming a bulk Lorentz factor of 100 and a redshift of 1, together with the cosmological parameters of $\Omega_m = 0.27$, $\Omega_\Lambda = 0.73$,

and $H_0 = 71\,\mathrm{km\,s^{-1}\,Mpc^{-1}}$, the photospheric radius was calculated as

$$R_{\rm ph} = 1.5 \times 10^{13}\ \mathrm{cm} \left(\frac{\gamma_0}{100}\right) \left(\frac{d_{\rm L}}{2.0 \times 10^{28}\ \mathrm{cm}}\right) \left(\frac{1+z}{2}\right)^{-2} \times \left(\frac{\mathcal{R}}{2.9 \times 10^{-17}}\right). \quad (1)$$

The radius of the main burst emission site was estimated by the 45 s delay which we observed between the MAXI/GSC and the CGBM data. The difference of the arrival time of the photons emitted between R_0 and aR_0 ($a > 1$) to the observers can be expressed as the radial time scale (Piran 1999), $\Delta T = [(a^4 - 1)/4](R_0/2\gamma_0^2 c)$, where γ_0 is the bulk Lorentz factor at R_0 and c is the speed of light. Substituting ΔT as the observed delay time $\Delta T_{\rm obs}$ of 45 s [$\Delta T = \Delta T_{\rm obs}/(1+z)$] and R_0 as the derived photospheric radius of 1.5×10^{13} cm, the parameter a was estimated as

$$a \sim 8 \left(\frac{\Delta T_{\rm obs}}{45\ \mathrm{s}}\right)^{\frac{1}{4}} \left(\frac{1+z}{2}\right)^{-\frac{1}{4}} \left(\frac{\gamma_0}{100}\right)^{\frac{1}{2}} \left(\frac{R_{\rm ph}}{1.5 \times 10^{13}\ \mathrm{cm}}\right)^{-\frac{1}{4}}. \quad (2)$$

Since the radius to the main burst episode site is $aR_{\rm ph}$, its radius was estimated to be $\sim 1.2 \times 10^{14}$ cm. This estimated radius is consistent with the radius between internal shocks in the case of $\gamma_0 = 100$ (Piran 1999). Note, however, that our discussion relies on the assumption concerning the redshift. Unfortunately, the sky location of GRB 160107A at the time of the trigger was too close to the Sun to perform follow-up observations from ground facilities. As shown here for GRB 160107A, the soft X-ray data of MAXI can provide an important clue in understanding the prompt emission from GRBs. Therefore, we strongly encourage follow-up to MAXI-detected GRBs to identify an afterglow and a host galaxy in order to determine a secure redshift measurement.

A possible origin of a thermal component is an emission from a mildly relativistic cocoon around a jet (Ramirez-Ruis et al. 2002; Nakar & Piran 2017). According to the calculation of Lazzati et al. (2017), the X-ray flux expected from a cocoon is $\sim 10^{-14}$–10^{-12} erg cm^{-2} s^{-1} at a typical distance of 1 Gpc for long GRBs. Our detected thermal X-ray emission was 8×10^{-9} erg cm^{-2} s^{-1}, which is two orders of magnitude brighter than the calculation. Another interesting possibility is a supernova shock breakout emission. The onset X-ray emission of a shock breakout was detected by Swift XRT for SN 2008D (Soderberg et al. 2008). The peak X-ray luminosity of this shock breakout was 6×10^{43} erg s^{-1}, which corresponds to 5×10^{-13} erg cm^{-2} s^{-1} at 1 Gpc. This estimated flux is three orders of magnitude weaker than the thermal emission of GRB 160107A. Therefore, either a cocoon or a shock breakout emission is expected to be below the detection sensitivity of MAXI/GSC at the typical distance of long GRBs, and is difficult to confirm as the origin of the thermal emission of GRB 160107A.

The blackbody temperature of 1 keV seen in the GRB 160107A spectrum is one or two orders of magnitude smaller than the reported blackbody temperature in the BATSE (e.g., Ryde 2005) and Fermi-GBM (e.g., Ryde 2010; Guiriec et al. 2013) GRB spectra. Our temperature is more consistent with the identified blackbody components reported by HETE-2 (Shirasaki et al. 2008) and Swift (Starling et al. 2012). However, our understanding of the thermal emission in the prompt GRB spectrum is limited by a small number of incomplete (e.g, no redshift measurement) samples. As we demonstrated here for GRB 160107A, the coordination of the scientific instruments onboard ISS becomes important to enhance the science outcome. Joint observation by ongoing X-ray missions like MAXI and NICER, and a future mission like TAO-ISS along with a hard X-ray survey instrument like CGBM will be crucial to collect high-quality broad-band data related to GRB emission.

Acknowledgments

We would like to thank the anonymous referee for comments and suggestions that materially improved the paper. We would also like to thank D. Svinkin for providing the analysis of the IPN localization, and also useful comments and discussions. We gratefully acknowledge JAXA's contributions in CALET development and on-orbit operations. We express our sincere thanks to all of the CALET members for allowing us to use the CGBM data. The CALET data used in this analysis are provided by the Waseda CALET Operation Center (WCOC) located at the Waseda University. This work is supported by MEXT KAKENHI Grant Numbers 17H06357, 17H06362 (T.S.), and 24684015 (K.Y.). This research was also supported by a grant from the Hayakawa Satio Fund awarded by the Astronomical Society of Japan (Y.K.).

Appendix 1. Energy response function of CGBM

The CGBM energy response function was built by a simulator based on the GEANT4 simulation package (Agostinelli et al. 2003). All the materials of the flight CGBM detectors are modeled in the simulator. The entire CALET structure is included in the simulator, although a simplified structure is used for the CAL (only precisely modeling the heavy elements which are responsible for the absorption and the scattering) in order to reduce the calculation speed (Yamada et al. 2017). The detailed instrumental characteristics of HXM and SGM, based on the results of the pre-flight ground testing (Nakahira 2017), are also included in the simulator.

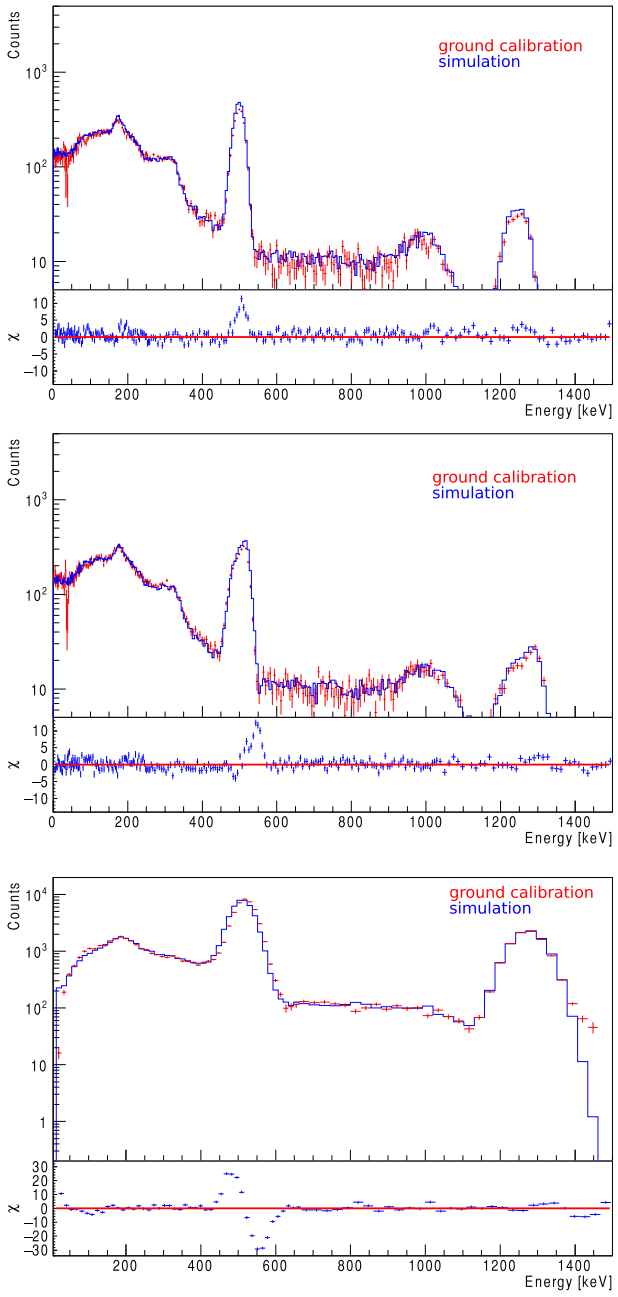

Fig. 7. Ground calibration (red) and the simulated (blue) spectra of ^{22}Na. The top, middle, and bottom panels show the spectra of HXM1, HXM2, and SGM, respectively. (Color online)

Ground testing data were collected by irradiating the flight instruments with radioactive sources and soft X-rays from an X-ray generator. Figure 7 shows a comparison between the data and the simulated ^{22}Na spectra for HXM1, HXM2, and SGM using the CGBM simulator. As can be seen in the figure, both the energies and the normalizations of the 511 keV and 1275 keV lines agree quite well. The difference in the line shape of the 511 keV line between HXM1 and HXM2 is also well modeled in the simulator. Despite a clear residual in the 511 keV line in the SGM, the overall shape of the spectrum shows good agreement. The net counts in the 511 keV peak in the simulated spectra are 20% and 3% larger than the calibration data of HXM and SGM, respectively. The energy resolution of the simulated spectra agrees with the measured value to within 5% for all detectors. Therefore, the CGBM simulator has been demonstrated to reproduce the ground testing data accurately.

Appendix 2. Spectral cross-calibration between CGBM and Swift/BAT using simultaneously detected bright GRBs

We used the bright GRBs simultaneously detected by the Swift/BAT since the systematic error in the energy response function has been studied in detail for Wind/KONUS and Suzaku/WAM using GRB data (Sakamoto et al. 2011). We identified two GRBs, GRB 161218A and GRB 170330A, for this investigation. The incident angles to the HXM and the SGM boresights are 37° and 30° for GRB 161218A, and 32° and 35° for GRB 170330A. We extracted time-averaged spectra for both the CGBM and the BAT using exactly the same time interval. The BAT spectrum was extracted from the event data using the standard procedure (C. B. Markwardt et al. 2007).[2] As was done in the spectral analysis of GRB 160107A, XSPEC (v12.9.1) was used in this joint spectral analysis.

First, we performed the joint spectral analysis only using the HXM data to focus on the investigation of the low-energy response of the HXM. The HXM spectrum was fitted between 30 and 150 keV. Figure 8 shows the joint fit spectra, and table 3 summarizes the best-fit parameters. Both the photon indices and the normalizations measured by the HXM are consistent with those measured by Swift/BAT. Also, no significant residual was seen in both joint fitted spectra of GRB 161218A and GRB 170330A. Therefore, we concluded that the systematic error in the low-energy part of the HXM data (30–150 keV) was 10%–20%, as discussed in Sakamoto et al. (2011) as the systematic uncertainty in the Swift BAT data.

Second, we included the SGM data in the fit. In this three-instrument joint fit, we multiplied the model by a constant factor. We fixed the constant factor of BAT to unity. Figure 9 shows the joint fit spectra and table 4 summarizes the joint fits by different spectral models. In the joint fitted spectra of GRB 161218A and GRB 170330A, the constant factors of HXM1 and HXM2 were consistent with unity, as is the case without the SGM data. The centroids of the SGM constant factors of GRB 161218A and GRB 170330A were

[2]C. B. Markwardt et al. 2007, The SWIFT BAT Software Guide ⟨https://swift.gsfc.nasa.gov/analysis/bat_swguide_v6_3.pdf⟩.

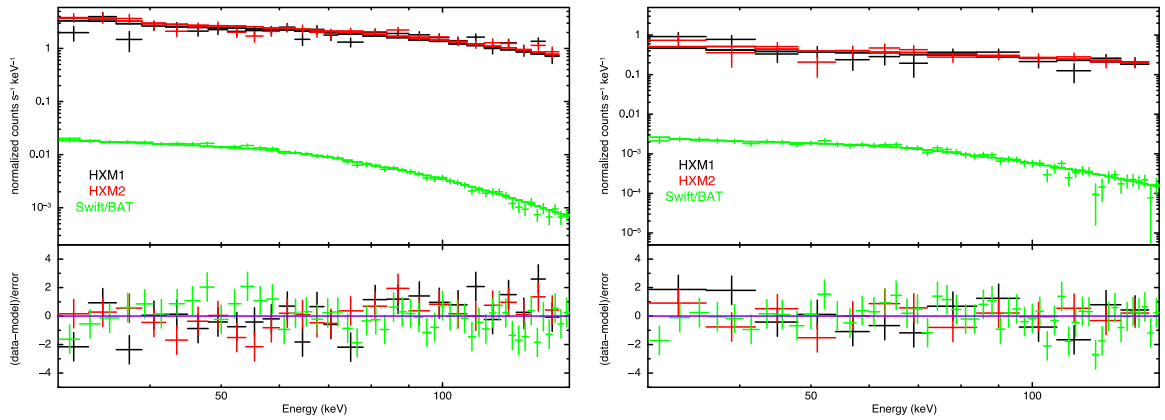

Fig. 8. Joint CGBM–Swift/BAT fitted spectra of GRB 161218A and GRB 170330A in the 30–150 keV band. The left panel shows the GRB161218A spectrum with a best-fit CPL model. The right panel shows the GRB 170330A spectrum and a best-fit PL model. The black, red, and green points are the HXM1, HXM2, and Swift/BAT data, respectively. (Color online)

Table 3. Fit parameters of GRB 161218A and GRB 170330A with HXM and Swift/BAT.

GRB name	Instrument	Models	C(HXM1)*	C(HXM2)†	α	$E_{\rm peak}$ [keV]	Norm [ph cm^{-2} s^{-1} keV^{-1}]	χ^2/ d.o.f.
GRB161218A	CGBM	CPL‡	–	–	$-0.95^{+0.63}_{-0.33}$	Not determined	$3.6^{+10.0}_{-2.8}$	44.75/49
	Swift/BAT	CPL	–	–	-0.67 ± 0.24	127^{+28}_{-15}	$2.1^{+2.4}_{-1.1}$	33.95/48
	Joint	CPL	$1.01^{+0.07}_{-0.06}$	0.98 ± 0.07	-0.98 ± 0.23	193^{+162}_{-45}	$5.4^{+5.8}_{-2.8}$	106.15/98
GRB170330A	CGBM	PL§	–	–	-1.22 ± 0.25	–	$1.5^{+3.1}_{-1.1}$	22.97/24
	Swift/BAT	PL	–	–	-1.17 ± 0.09	–	$1.16^{+0.50}_{-0.35}$	42.11/49
	Joint	PL	0.95 ± 0.14	1.04 ± 0.15	-1.17 ± 0.08	–	$1.18^{+0.48}_{-0.34}$	64.52/73

*A constant factor of HXM1.
†A constant factor of HXM2.
‡A power law times exponential cutoff model.
§A power-law model.

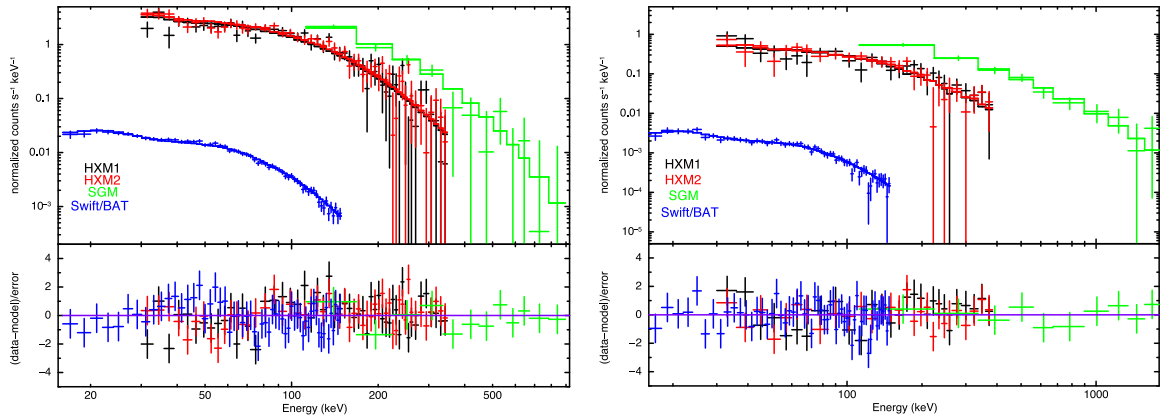

Fig. 9. Joint CGBM–Swift/BAT fitted spectra of GRB 161218A and GRB 170330A including the SGM data. The left panel shows the GRB 161218A spectrum with a CPL model. The right panel shows the GRB 170330A spectrum with a CPL model. The black, red, green, and blue points are the HXM1, HXM2, SGM, and Swift/BAT data. (Color online)

1.3 and 1.8, probably due to the incomplete modeling of the CALET in the simulator. Furthermore, the time-dependent background variation due to charged particles makes it difficult to model the background spectrum accurately. Since we are still working on understanding the influence of the structures around the detector and the uncertainty in the background modeling, we decided to multiply the model by a constant factor as a free parameter in the GRB 160107A

Table 4. Fit parameters of GRB 161218A and GRB 170330A from joint fit with HXM, SGM, and Swift/BAT.

GRB name	Models	C(HXM1)*	C(HXM2)†	C(SGM)‡	α	β	$E_{\rm peak}$ [keV]	Norm [ph cm^{-2} s^{-1} keV^{-1}]	χ^2/ d.o.f.
GRB161218A	PL§	0.87 ± 0.06	0.93 ± 0.06	0.37 ± 0.06	-1.36 ± 0.03	–	–	17 ± 2	556.90/171
	CPL‖	1.03 ± 0.06	1.09 ± 0.06	$1.25^{+0.14}_{-0.13}$	$-0.69^{+0.09}_{-0.08}$	–	148^{+13}_{-11}	$2.1^{+0.6}_{-0.5}$	164.92/170
	BAND#	1.01 ± 0.06	1.08 ± 0.06	1.10 ± 0.12	$-0.62^{+0.11}_{-0.12}$	-2.3 (fixed)	136^{+14}_{-12}	$0.10^{+0.02}_{-0.01}$	194.67/170
GRB170330A	PL	$1.06^{+0.14}_{-0.13}$	$1.10^{+0.15}_{-0.14}$	$0.99^{+0.20}_{-0.18}$	-1.25 ± 0.05	–	–	$1.6^{+0.4}_{-0.3}$	169.79/119
	CPL	$1.09^{+0.14}_{-0.13}$	1.14 ± 0.14	$1.82^{+0.29}_{-0.26}$	-0.98 ± 0.08	–	463^{+123}_{-87}	$0.63^{+0.22}_{-0.17}$	93.03/118
	BAND	$1.09^{+0.14}_{-0.13}$	1.14 ± 0.14	$1.84^{+0.31}_{-0.27}$	$-0.97^{+0.10}_{-0.09}$	-2.3 (fixed)	423^{+129}_{-95}	$6.9^{+0.8}_{-0.6} \times 10^{-3}$	93.07/118

*A constant factor of HXM1.
†A constant factor of HXM2.
‡A constant factor of SGM.
§A power-law model.
‖A power law times exponential cutoff model.
#Band function.

data to take into account the currently unknown systematic uncertainty in the SGM data.

References

Abbott, B. P., et al. 2016, Phys. Rev. Lett., 116, 061102
Abbott, B. P., et al. 2017, ApJ, 848, L12
Agostinelli, S., et al. 2003, Nucl. Instrum. Methods Phys. Res., Sect. A, 506, 250
Amati, L., et al. 2002, A&A, 390, 81
Band, D., et al. 1993, ApJ, 413, 281
Connaughton, V., et al. 2015, ApJS, 216, 32
Dickey, J. M., & Lockman, F. J. 1990, ARA&A, 28, 215
Eichler, D., Livio, M., Piran, T., & Schramm, D. N. 1989, Nature, 340, 126
Frontera, F., et al. 2001, ApJ, 550, L47
Golenetskii, S., et al. 2016, GCN Circ., 18857
Goodman, J. 1986, ApJ, 308, L47
Gruber, D., et al. 2014, ApJS, 211, 12
Guiriec, S., et al. 2013, ApJ, 770, 32
Kaneko, Y., Preece, R. D., Briggs, M. S., Paciesas, W. S., Meegan, C. A., & Band, D. L. 2006, ApJS, 166, 298
Kouveliotou, C., Meegan, C. A., Fishman, G. J., Bhat, N. P., Briggs, M. S., Koshut, T. M., Paciesas, W. S., & Pendleton, G. N. 1993, ApJ, 413, L101
Lazzati, D., Deich, A., Morsony, B. J., & Workman, J. C. 2017, MNRAS, 471, 1652
Matsuoka, M., et al. 2009, PASJ, 61, 999
Nakagawa, Y. E., et al. 2016, GCN Circ., 18839
Nakahira, S., 2017, in Proc. 7 years of MAXI: Monitoring X-ray Transients (Wako: RIKEN), 261
Nakahira, S., et al. 2016, GCN Circ., 18845
Nakar, E., & Piran, T. 2017, ApJ, 834, 28
Narayan, R., Paczynski, B., & Piran, T. 1992, ApJ, 395, L83
Narayana Bhat, P., et al. 2016, ApJS, 223, 28
Ono, Y., et al. 2016, GCN Circ., 19404, 1
Paczynski, B. 1986, ApJ, 308, L43
Paczynski, B. 1991, Acta Astron., 41, 257
Pe'er, A., Ryde, F., Wijers, R. A. M. J., Mészáros, P., & Rees, M. J. 2007, ApJ, 664, L1
Piran, T. 1999, Phys. Rep., 314, 575
Preece, R. D., Briggs, M. S., Mallozzi, R. S., Pendleton, G. N., Paciesas, W. S., & Band, D. L. 1998, ApJ, 506, L23
Quarati, F. G. A., Khodyuk, I. V., van Eijk, C. W. E., Quarati, P., & Dorenbos, P. 2012, Nucl. Instrum. Methods Phys. Res., Sect. A, 683, 46
Ramirez-Ruiz, E., Celotti, A., & Rees, M. J. 2002, MNRAS, 337, 1349
Ryde, F. 2005, ApJ, 625, L95
Ryde, F., et al. 2010, ApJ, 709, L172
Sakamoto, T., et al. 2005, ApJ, 629, 311
Sakamoto, T., et al. 2011, PASJ, 63, 215
Shirasaki, Y., et al. 2008, PASJ, 60, 919
Soderberg, A. M., et al. 2008, Nature, 453, 469
Starling, R. L. C., Page, K. L., Pe'er, A., Beardmore, A. P., & Osborne, J. P. 2012, MNRAS, 427, 2950
Sugizaki, M., et al. 2011, PASJ, 63, S635
Tamura, T., Baba, H., Matsuzaki, K., Miura, A., Shinohara, I., Nagase, F., Fukushi, M., & Uchida, K. 2004, in ASP Conf. Ser., 314, Astronomical Data Analysis Software and Systems (ADASS) XIII, ed. F. Ochsenbein et al. (San Francisco: ASP), 22
Tavani, M. 1996, ApJ, 466, 768
Torii, S., & CALET Collaboration, 2011, Nucl. Instrum. Methods Phys. Res., Sect. A, 630, 55
Veres, P., & Meegan, C. 2016, GCN Circ., 18844, 1
von Kienlin, A., et al. 2014, ApJS, 211, 13
Willingale, R., Starling, R. L. C., Beardmore, A. P., Tanvir, N. R., & O'Brien, P. T. 2013, MNRAS, 431, 394
Woosley, S. E., & Bloom, J. S. 2006, ARA&A, 44, 507
Yamada, Y., Sakamoto, T., & Yoshida, A. 2017, in Proc. 7 years of MAXI: Monitoring X-ray Transients (Wako: RIKEN), 271
Yamaoka, K., et al. 2013, in Proc. 7th Huntsville Gamma-Ray Burst Symposium, GRB 2013, r 41 in eConf Proceedings C1304143 (arXiv:1311.4084)